A THREE DEGREE OF FREEDOM
MICRO-MOTION IN-PARALLEL ACTUATED MANIPULATOR

Kok-Meng Lee
Assistant Professor

Shankar Arjunan
Senior Engineer

Georgia Institute of Technology
Atlanta, GA 30332

Cummins Engine Company, Ltd.
Columbus, IN 47203

ABSTRACT

The advancement of micro-miniaturization and other emerging technologies in the world of microns .has motivated the search for a technique that will permit precision manipulation control. This paper presents the development of a three degree of freedom (DOF) micro-motion in-parallel actuated manipulator, which has one translation and two orientation freedoms. The micro-motion manipulation is achieved by means of piezo-electric effects due to its fast response and high resolution. In particular, the paper presents a closed-form solution and an experimental verification of the forward kinematics. In addition, the dynamic model of the piezo-electric actuated link was determined experimentally, which provides a rational basis for the design and prismatic joint force control of the high speed micro-motion manipulator. A special configuration which approaches an optimal design, in terms of working range, rigidity, and bandwidth, is highlighted.

1. INTRODUCTION

The concept of micro-miniaturization has had a revolutionary impact on electronics and has indicated the benefits of extending it to other fields such as integrated optics [1-4]. These impacts are attributed to the advantages of reduced weight and volume, lower power consumption, and gain in ruggedness and speed of response. Lebet [5] has further included the assembly of optical components and delicate mechanical devices as potential application areas of micro-engineering. The advancement of micro-miniaturization and other merging technologies in the world of microns has motivated the search for a technique that will permit high-speed precision manipulation.

Industrial robots have well been recognized to have limited static accuracy for micro-miniaturization applications due to the measurement errors, poor rigidity, and non-linearities of the actuators. The design of a series-parallel micro-motion mechanism was proposed as a wrist torque sensor and to enhance the resolution of an innovative spherical motor [6] [7], which is characterized by its singular-free kinematics within its workspace and by its attractive possibility of combining the roll, pitch and yaw motions in a single joint.

This paper presents the development of a three DOF micro-motion in-parallel actuated manipulator which has two orientation and one translation freedoms. The inverse kinematics and dynamics of the mechanism as a coarse motion manipulator were discussed by Lee and Shah [8] [9]. This paper focuses on the closed-form solution and experimental verification of the forward kinematics for micro-motion control. To provide a rational basis for the control of high-speed micro-motion manipulation using piezo-electric actuation, the dynamic model of a micro-motion manipulator was determined experimentally.

2. LINEARIZED FORWARD KINEMATICS

A schematics of a three DOF in-parallel actuated manipulator is shown in Fig. 1, where the moving platform can be manipulated with respect to the base platform by varying the link lengths.
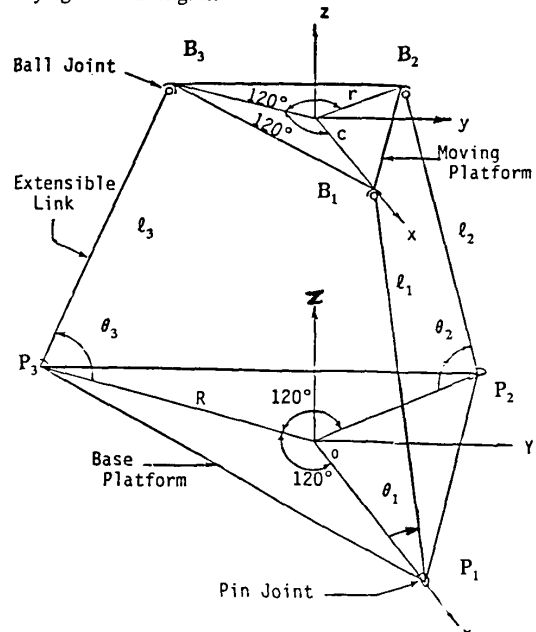

Fig.1 A 3-DOF In-Parallel Actuated Manipulator

The coordinate system is shown in Fig. 1. A base coordinate frame XYZ, with unit vectors $\underline{i}$, $\underline{j}$, and $\underline{k}$ respectively, is fixed at the center of the base platform with the Z axis pointing vertically upward and the X axis pointing towards pin joint, P_1. Similarly, coordinate frame xyz is assigned to the center of the movable platform with the z axis normal to the platform and the x axis pointing toward the ball joint, indicated as B_1.

As the distance between the adjacent ball joints or the ith and j^{th} links is $r\sqrt{3}$, the implicit relationship between the link lengths and the subtended angles is [8]:

$$L_i^2 + L_j^2 + 3 - 3\rho^2 + L_i L_j \cos\theta_i \cos\theta_j$$
$$- 2L_i L_j \sin\theta_i \sin\theta_j - 3L_i \cos\theta_i - 3L_j \cos\theta_j = 0 \quad (1)$$

where $i = 1, 2, 3$ and $j = 2, 3, 1$, and where $L_i = \ell_i/R$ and $\rho = r/R$. Equation (1) is of the form $f_i(\theta_i, \theta_j, L_i, L_j) = 0$. The motion is in the order of microns and thus, can be linearized about an operating point, $\theta_i = \theta_o$ and $L_i = L_o$. For a specified L_o, the corresponding operating angle θ_o is determined from the geometry; i.e.

$$\cos\theta_o = R(1 - \rho) / L_o$$

By expanding $f_i(\theta_i, \theta_j, L_i, L_j)$ in a Taylor series and noting that

$$\left.\frac{\partial f_i}{\partial\theta_i}\right|_{\theta_o, L_o} = \left.\frac{\partial f_i}{\partial\theta_j}\right|_{\theta_o, L_o} = c_1$$

and

$$\left.\frac{\partial f_i}{\partial L_i}\right|_{\theta_o, L_o} = \left.\frac{\partial f_i}{\partial L_j}\right|_{\theta_o, L_o} = c_2$$

where

$$c_1 = 3 L_o \sin\theta_o [1 - L_o\cos\theta_o]$$

$$c_2 = -3 \cos\theta_o [1 - L_o\cos\theta_o]$$

the linearized equation about an operating point (θ_o, L_o) is

$$\Delta\theta_i + \Delta\theta_j = -\frac{c_2}{c_1}(\Delta L_i + \Delta L_j) \quad (2)$$

where $\Delta\theta = \theta - \theta_o$ and $\Delta L = L - L_o$ and the subscripts denote the respective links $i = 1, 2, 3$ and $j = 2, 3, 1$. $\Delta\theta_i$ can be derived by solving the three constraint equations simultaneously:

$$\Delta\theta_i = \frac{\Delta L_i}{L_o \tan\theta_o} \quad (3)$$

where $\tan\theta_o \neq 0$. The three linearized equations, i.e. Equation (3) with $i = 1, 2, 3$, are decoupled. It is worth noting that when $\theta_o = \pi/2$, and the change in link length is accompanied with no change in the subtended angle.

Cartesian position of moving platform

By noting that the origin of the xyz frame is essentially the centroid of the triangle formed by joining the three ball joints, the center of the moving platform is at

$$X_c = \frac{1}{3}\sum_{i=1}^{3} L_i \cos\theta_i \cos[\frac{2}{3}(i-1)\pi] \quad (4a)$$

$$Y_c = \frac{1}{3}\sum_{i=1}^{3} L_i \cos\theta_i \sin[\frac{2}{3}(i-1)\pi] \quad (4b)$$

$$Z_c = \frac{1}{3}\sum_{i=1}^{3} L_i \sin\theta_i \quad (4c)$$

Orientation of moving platform

With the coordinates of the ball joints described in terms of the link lengths and the subtended angles, the unit vectors of the body axes xyz with respect to the base coordinate XYZ are given as follows:

$$\underline{u}_x = \frac{\overrightarrow{OB_1} - \overrightarrow{OC}}{r}, \qquad \underline{u}_y = \frac{\overrightarrow{OB_2} - \overrightarrow{OB_3}}{\sqrt{3}\,r}$$

and

$$\underline{u}_z = \underline{u}_x \times \underline{u}_y \quad (5)$$

where OB_i is the line vector originated from the point O to the center of the ith ball joint, and OC is the line vector originated from the point O to the center of moving platform C.

The orientation will be described in terms of the rotation about the X and Y axes of the base coordinate designated as α and β respectively. The transformation matrix, which describes the coordinate transformation of the xyz body axes with respect to the base coordinate XYZ, is given by

$$[ROT] = \begin{vmatrix} \cos\beta & \sin\beta\sin\alpha & \sin\beta\cos\alpha \\ 0 & \cos\alpha & -\sin\alpha \\ -\sin\beta & \cos\beta\sin\alpha & \cos\beta\cos\alpha \end{vmatrix} \quad (6)$$

The matrix [ROT] is equal to $[\underline{u}_x\ \underline{u}_y\ \underline{u}_z]$.

From Equations (5) and (6), the angles α and β can be obtained by the following relations:

$$\alpha = \tan^{-1}\left(u_{yk}/u_{zk}\right) \quad (7a)$$

$$\beta = \tan^{-1}\left(u_{zi}/u_{zk}\right) \quad (7b)$$

and the angle of rotation about z-axis is

$$\gamma = \cos^{-1}u_{xi} \quad (7c)$$

The forward kinematics can be computed as follows: First, the change of subtended angle, $\Delta\theta_i$, is determined using Equation (3). The cartesian position of the moving platform is then computed using Equation (4), and the

1699

angles of rotation about X and Y axes α and β from Equations (7a)-(7b) with the unit vectors of the body axes defined in Equation (5).

3. PROTOTYPE MICRO-MOTION MANIPULATOR

The design of a prototype manipulator is shown in Fig. 2. The prototype links which have the motion in the order of microns were actuated by a piezo-electric actuator as shown in Fig. 2(a). All components were assembled and tight fixed by means of solid pins in order to eliminate any possible relative motion.

The link design consists of a cantilever structure which flex at a pivot points A and the actuation is provided at Q. The cantilever structure is to enable an amplification of the motion generated by the piezo-electric actuator located at Q. The piezo-electric element was clamped between the base and the compressor. The loader which behaves as a rotational spring is to ensure a positive contact between the actuator and the link. The equivalent change in the link length, ΔL, and the subtended $\Delta\theta$, of the prototype link design can be derived by regarding point P as a virtual pin joint. The argument is substantiated as shown in Fig. 3 where the point P is the initial position and the point P' is the corresponding position after the cantilever has been actuated by the piezo-electric actuator at Q. Similarly the point B has been moved to B_1 after the actuation. Hence the angle that is subtended between lines PB and PB_1 is the angle of rotation about the virtual joint P. The effective change in link length, PB_1 - PB, is derived as follows: Length PB_1 can be derived by applying the law of cosines to the triangle PP'B_1 shown in Fig. 3.

$$PB_1^2 = PB^2 + (PP')^2 + 2(PB)(PP')\sin\theta_0$$

From geometry, the deflection at P, PP', is approximated as $(b/c)y_q$ where y_q is displacement at Q.

$$\left[\frac{PB_1}{PB}\right]^2 = 1 + 2\frac{b}{c}\frac{y_q}{a}\sin\theta_0 + (\frac{b}{c}\frac{y_q}{a})^2$$

where a, b and c are the lengths PB, QP and AQ respectively. Neglecting the higher order terms of $(b/ac)y_q$, the change in link length is:

$$\Delta L = PB_1 - PB = \frac{b}{c}y_q\sin\theta_0 \tag{8}$$

The underlying assumption of Equation (8) is that the geometry $2by_q/(ac)$ must be smaller than unity. Hence, the prototype link design has a virtual pin joint at P and has an effective change in link length given in Equation (8).

The function of the ball joint, as shown in Fig. 2(b), is to provide the three rotational degrees of freedom. The thin cylindrical cross-section at A allows bending about the x and y axes. The thin section at C enables the rotation about the Z axis as seen in the figure. The neutral axes are BN for bending about the x and y axes and ND for the bending about z axis respectively. The length of the vector BD, which connects the point B and
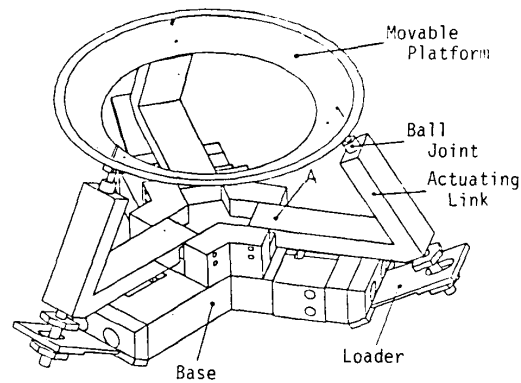

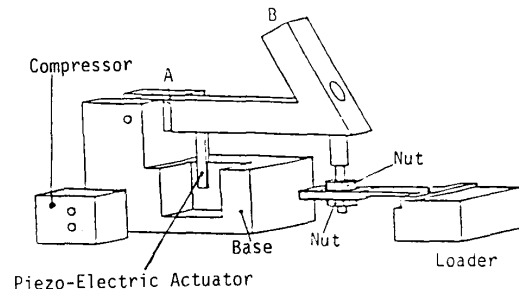Fig.2 Prototype Micro-Motion Manipulator
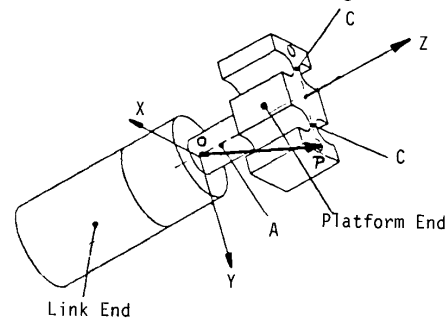

Fig.2(a) Prototype Link Design
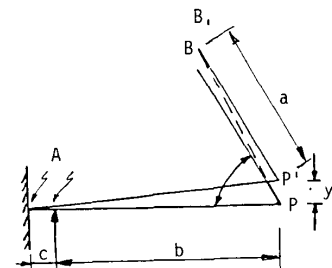

Fig.2(b) Prototype Ball Joint Design

Fig.3 Virtual Pin Joint

1700

the pin location D remains a constant. Hence, the structure has a virtual ball joint with its center at B and an effective radius equal to BD. The ball joint was rigidly attached to the movable platform at D, which was constructed in the shape of the frustum of a cone as shown in Fig. 2.

The parameters of the link and the specifications of the piezo-electric actuator are listed in TABLE 1. The piezo-electric element used in the experiment was TOKIN 2x3x18 [10], where the numerical value are the physical dimensions in mm. The piezo-electric element has a linear range of 0-15μm corresponding to 0-150 volts input.

TABLE 1 - Piezo-Electric Actuated Link Parameters

Piezo-Electric :	TOKIN NLA 2x3x18
Maximum Travel :	10μm
Force Generation :	350Kg/cm^2
Link Geometry :	b = 50mm, c = 5mm,
	a = 63mm, θ = 60°
Aluminum Cross Section :	10mm x 13.5mm
Pin Cross Section :	0.508mm x 13.5mm

3.1 Experimental Results of Kinematics

To verify the kinematics of the micro-motion manipulator, a mirror was attached to the movable platform. A laser beam was directed towards the mirror reflected on the wall at a distance of about 9 meters (30 feet). From the correlation between the beam deflection and the angle of rotation of the moving platform, the kinematics were determined and verified.

Correlation Between Experiments and Analysis

The following steps were taken to correlate the experimental data to the forward kinematics. When the beam is directed to the center of the moving platform, denoted as C, it reflects from position A_1 to A_2 as shown in Fig. 4. Consider the triangle CA_1A_2, where ϕ is the angle of rotation reflected by the laser beam. From the geometry, the angle, ϕ, can be determined as $\tan^{-1}(A_1A_2/CA_1)$ where A_1A_2 is beam deflection on the wall to be measured experimentally and CA_1 is predetermined distance of 9 meters. It is known from the law of physics that when the reflected beam travels through ϕ, the mirror should have rotated through $\phi/2$. Hence, the angle of rotation can be inferred from the measured distance of the beam before and after moving the link.

Since link 1 is located in the Y = 0 plane, the platform will rotate only about the Y axis if only link 1 is actuated. Hence there is a direct correlation between the angle of rotation about the y-axis, and the angle of rotation of the reflected beam determined from experiment. However, if only link 2 or link 3 is actuated, the plate will rotates about the line joining ball joints B_1 and B_3. By constructing the vectors directed from the mid-point between B_1 and B_3, to the point C, before and after the motion of link 2
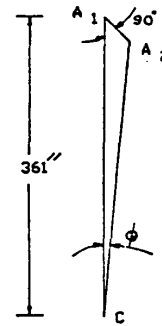

Fig.4 Determination of Rotation Angle

or link 3, it can be deduced that the angle between these two vectors is essentially the angle of rotation of the moving platform. For an input of 100 volts to one of the links, the image of the beam moved a distance of 6.25mm (0.25 inch). The points were half-way for an input of 50 volts, and thus verified that the motion is linear within the range tested. As the beam deflection was rather insensitive to z-displacement, no attempt was made to measure the z-motion directly.

The end-point position for the link actuation were determined by the linearized forward kinematic where the changes in link length were measured by the strain gages. The results are summarized in TABLE 2. The analytical results show good agreement with the experimental data. The steady state end-point position/orientation of the micro-motion manipulator can be determined rather accurately from the linearized closed-form forward kinematics.

TABLE 2 - Experimental Data

LINK ACTUATION	ANGLE OF ROTATION	
	Experimental	Analytical
Link 1	-0.02142°	-0.0227°
		α = 0, β = -0.0227°
Link 2	0.02539°	0.02806°
		α = 0.0247°, β = 0.0143°
Link 3	0.01983	0.02099°
		α = -0.0187°, β = 0.01496°

3.2 Dynamic Model of Actuating Link

The dynamic effects of the moving platform and the payload on the individual link control can be considered as reaction forces acting at the ball joints. It is of interest to determine the dynamic model of the link actuated by the piezo-electric element. The dynamic model was obtained experimentally using the standard frequency response technique with a HP3562A dynamic analyzer. The experimental set-up is shown in Fig. 5. The output signal of the HP analyzer was fed to a KEPCO power

1701

amplifier with a gain of 10, which in turn drove the piezo-electric actuator. The voltage output from the bridge is fed into a ANALOG DEVICES 3B18 signal conditioning amplifier for filtering and signal amplification. The conversion factor of combined strain gage calibration and 3B18 amplification was 1.3 volt/mm.
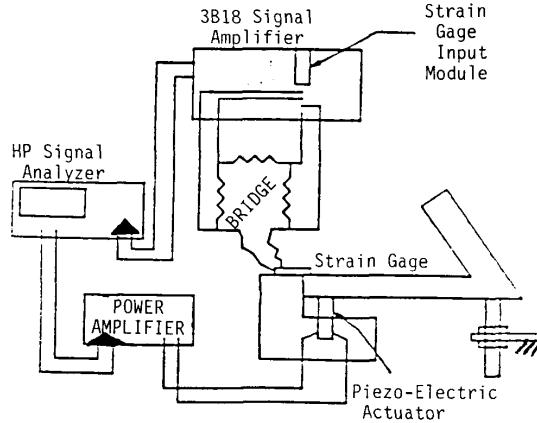
Fig.5 Experimental Setup

The Bode plots obtained experimentally to model the link dynamics are displayed in Fig. 6. The experimentally determined transfer function is

$$\frac{Y_q(s)}{V(s)} = K \prod_{i=1}^{3} \frac{s^2 + a_{1i}s + a_{0i}}{s^2 + b_{1i}s + b_{0i}} \qquad (9)$$

where K = 5.93 E-5

a_{01} = 1.97 E+6	a_{02} = 2.24 E+7	a_{03} = 6.63 E+7
a_{11} = 110	a_{12} = 2009	a_{13} = 1005

and

b_{01} = 1.06 E+6	b_{02} = 9.51 E+6	b_{03} = 2.23 E+7
b_{11} = 110	b_{12} = 519	b_{13} = 235

and where s is a Laplacian operator, V(s) is the input voltage to the piezo-electric element, and $Y_q(s)$ is the displacement measured at Q in mm. To verify the transfer function of the link in time domain, a step input of 75 volts was applied to the actuator. The strain gage output data were sampled at 20 kHz digitally using an IBM PC/XT with a METRABYTE Dash-16 data acquisition hardware. The experimental and analytical data show good agreement and exhibited all the dynamics involved, as shown in Fig. 7. The two graphs do not match perfectly but they exhibit how the higher order frequencies are dominant in the response. The higher-order frequency components are due primarily to that of the piezo-electric elements.

4. SPECIAL CONFIGURATION

A special configuration corresponding to θ_o = 90° is worth noting. For θ_o = 90°, which implies R = r,
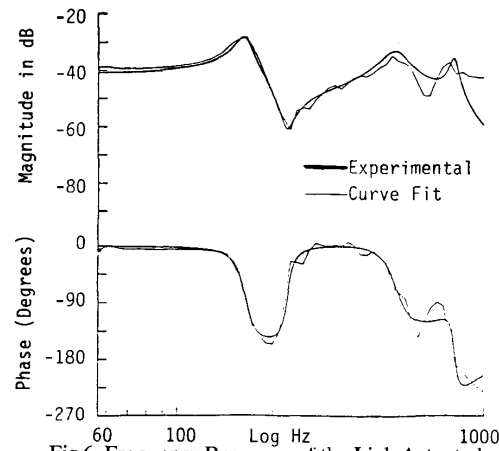
Fig.6 Frequency Response of the Link Actuated by Piezo-Electric Element
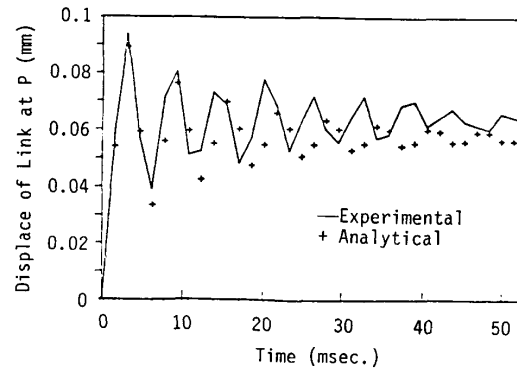
Fig.7 Open-Loop Step Response

Equation (3) indicates that a change in link length, ΔL_i, results in no change in subtended angle $\Delta\theta i$, as shown in Equation (3). It follows from the forward kinematic equations are:

$$X_c = Y_c = 0 \quad \text{and} \quad \Delta Z_c = \frac{1}{3}\sum_{i=1}^{3}\Delta L_i$$

$$\alpha = \frac{1}{\sqrt{3}}(\Delta L_2 - \Delta L_3), \quad \beta = \Delta L_1 - \Delta Z_c \text{ and } \gamma = 0 \quad (10)$$

The corresponding linearized inverse kinematics are:

$$\Delta L_1 = \Delta Z_c + \beta\cos\frac{2\pi}{3}(i-1) + \alpha\sin\frac{2\pi}{3}(i-1) \qquad (11)$$

The linearized forward and inverse kinematics are given in Equations (10) and (11) respectively. This special case, where θ_o = $\pi/2$ radians, indicates the micro-motion control of α, β, and Z_c can be achieved accompanied with no change in X_c, Y_c, and γ. The work-envelope is such that the maximum values of α and β decrease from a maximum at ΔZ_c = 0 to zero at ΔZ_c = ± Y_{max}. It is

1702

interesting to note that the kinematic is independent of ℓ_o.

From the principle of virtual work, it can be shown that the static force relationship between the Cartesian force vector acting at the moving platform, $[T_x/R, T_y/R, F_z]$ and the joint force vector $[F_1, F_2, F_3]$ is

$$\begin{bmatrix} F_1 \\ F_2 \\ F_3 \end{bmatrix} = \frac{1}{3} \begin{bmatrix} 0 & 2 & 1 \\ \sqrt{3} & -1 & 1 \\ -\sqrt{3} & -1 & 1 \end{bmatrix} \begin{bmatrix} T_x/R \\ T_y/R \\ F_z \end{bmatrix} \quad (12)$$

where F_i, $i = 1,2,3$, is the actuating force perpendicular to the moving platform through the ball joint; T_x, and T_y are the torques acting about X and Y axes and the force acting in the Z-direction respectively. F_i can be approximated as $(c/b) F_p$ where F_p is the force actuated by the piezo-electric elements. Hence, the measurements of F_i allow the Cartesian moment force vector to be determined by Equation (12).

In this particular configuration, the micro-motion manipulator provides the actuating torques about X- and Y- axes and an actuating force along the Z-direction. Any external moments about Z-axis, T_z, or external forces along X and Y axes, F_x and F_y must be supported by the joints in the form of reaction forces. The external forces, F_x and F_y, would result in bending moments equal to $F_x\ell_o$ and $F_y\ell_o$ on the links. However, as the range of motion is independent of ℓ_o in the $\theta_o = \pi/2$ configuration, the bending movements on the link can be reduced to a minimum or zero, using a design with minimum ℓ_o or $\ell_o = 0$ respectively. In addition, the possibility of reducing ℓ_o to a minimum or zero value has a potential to further increase the bandwidth of the manipulator.

5. CONCLUSION

The design concept of a three DOF micro-motion, in-parallel actuated manipulator using piezo-electric actuators has been examined and developed. The development has indicated that high-speed micro-motion manipulation can be achieved using piezo-electric actuation.

In particular, the closed-form kinematics for micro-motion manipulation have been derived and experimentally verified. A special configuration corresponding to $\theta = \pi/2$ would result in micro-motion control of α, β, and Z_c accompanied with no change in the subtended angles and, thus, no changes in X_c, Y_c, and γ. As the kinematics are independent of ℓ_o, the special configuration approaches an optimal design in terms of working range, rigidity and bandwidth. The static force relationship between the joint space and the task space is given, which is useful for three DOF force/torque sensing.

The dynamic model of the piezo-electric actuated link has been determined experimentally, which provides a rational basis for the design and for prismatic joint force control of the high-speed micro-motion manipulator. The studies have indicated that significant high-order

frequency components due to the piezo-electric actuation are present in the link dynamics.

REFERENCES

1. Blodgett, A. J. Jr., 1983, "Microelectronic packaging," Scientific American July.
2. Robinson, G. M., 1987, "How advanced motion control enhances cancer treatment," Design News Vol. 9-21-87.
3. Haugen, G. "Micro miniaturization is finding application beyond electronics," Research and Development, March 1987, pp. 66-69.
4. Taniguchi, N., 1983, "Current status in, and future trends of, ultraprecision machining and ultrafine materials processing," CIRP Annuals Vol. 32/2/83.
5. Lebet, P., "Assembly with robots in micro-engineering," International conference on assembly automation, 1982., pp. 29-40.
6. Lee K-M., Vachtsevanos G. and Kwan, C-K., 1988 "Development of a spherical stepper wrist motor," Proceedings of the 1988 IEEE International Conference of Robotics and Automation.
7. Lee, K-M. and Arjunan S., "Force/Torque Sensing and Micro-Motion Manipulator of a Spherical Stepper Wrist Motor," Proceedings of the 1988 ACC.
8. Lee, K-M and Shah, D., 1987, "Kinematic Analysis of a Three Degree of Freedom In-parallel Actuated Manipulator," Proceedings of the 1987 IEEE International Conference of Robotics and Automation. Also in IEEE Journal of Robotics and Automation, Vol. 4 Issue 2 June 1988.
9. Lee, K-M and Shah, D., 1988, "Dynamic Analysis of a Three Degree of Freedom In-parallel Actuated Manipulator," IEEE Journal of Robotics and Automation, Vol. 4. Issue 2.
10. Tokin manufacturer's booklet on multilayer piezo-electric actuators.